Chapter 2

Experimental details

In this chapter we provide the reader with a summary of some basic concepts we consider might be helpful for understanding the scientific discussion contained in the main chapters of this thesis. First, we briefly describe the phenomenon of adsorption and give some reasons to explain why the use of ultra-high-vacuum techniques had been so far necessary for the study of processes occurring at the surface of a solid. Then, we give some general notions about core level photoemission, in which the photoelectron diffraction technique is based. Afterwards, the photoelectron diffraction technique is described in some detail. This technique was used in its scanned-energy mode to determine the local adsorption structure of the three different adsorbate-substrate systems reported in this work. In order to have a 'light' source whose energy can be varied, we have utilised synchrotron radiation. Because of this, some aspects of what synchrotron radiation is and how it can be produced are also given in this chapter. Finally, we give some hints on what the low energy electron diffraction (LEED) technique is and on the different notations used to refer to the LEED patterns of ordered adsorbed overlayers.

2.1 Adsorption and the use of UHV

As mentioned in the introduction of this work, bond breaking associated with chemisorption on the surface of a catalyst is one of the key processes in heterogeneous catalysis. Atoms in a surface clearly differ from their bulk counterparts since they cannot interact symmetrically with neighbouring atoms. Due to that, they commonly exhibit unsaturated valencies that cause an attractive force normal to the surface plane and allow them to form bonds with foreign atoms or molecules on the surface. The term adsorption is used to define the accumulation of the so called adsorbate (from the gas phase) at the surface of a solid substrate or adsorbent. Depending on the strength of the interaction between adsorbate and substrate at the gas-solid interface, the adsorption process can be classified as *chemisorption* or *physisorption*. When a chemical interaction between the adsorbate and the substrate occurs, and a chemical bond is established between them, the adsorption phenomenon is called *chemisorption*. When the adsorbate is held to the surface by

means of van der Waals forces, then it is called *physisorption*. The dissociation of molecular oxygen into adsorbed atomic oxygen on various metals surfaces is a clear example of chemisorption; the interaction of the inactive rare gases on most substrates provides an example of physisorption.

Adsorption of a gas at the surface of a solid occurs spontaneously which in thermodynamical terms means that the free energy G of the gas/solid system in equilibrium is decreased. Moreover, since the adsorbed state is more ordered than the gaseous state, the entropy change is negative. Then, according to the expression:

$$\Delta H = \Delta G + T\Delta S \tag{2.1}$$

the enthalpy change associated with the adsorption phenomenon is also negative, i.e. adsorption is an exothermic process. The heat liberated during adsorption is called the *heat of adsorption* and its magnitude is frequently used as a criterion to distinguish between chemisorption and physisorption. The upper limit of the heat of adsorption for a physisorbed system is considered to be around 60 KJ mole^{-1} ($\sim$ 0.6 eV per atom or molecule). However, this value should not be considered as a rigid limit. In fact, there are weak chemisorbed systems (e.g. the N_2/Ni(100) system reported in this thesis) with heats of adsorption lower than that.

The initial step of adsorption involves the collision of the gaseous adsorbate with the surface. The rate of arrival of atoms or molecules of the gas per second and per cm^2 is given by the Herz-Knudsen equation:

$$r = P/(2\pi mkT)^{1/2} \tag{2.2}$$

where P is the gas pressure, m is the mass of the gaseous atom or molecule, T the temperature and k the Boltzmann constant. Of course not all the atoms or molecules arriving at the surface of the substrate stick to it. Therefore, the rate of adsorption differs from the rate of arrival by a factor called *sticking factor*, and the equation for the rate of adsorption can be written as follows:

$$r = s{\cdot}P/(2\pi mkT)^{1/2} \tag{2.3}$$

where s is the sticking factor or sticking probability. The sticking probability is influenced by a number of factors, as for instance the presence of unoccupied adequate adsorption sites. In general is a difficult task to determine the sticking factor in a direct way.

From the expressions 2.2 and 2.3 we can obtain a clear explanation of one of the reasons why the use of ultra-high-vacuum is helpful in order to study processes which occur at a surface of a solid. Our atmosphere contains around 74% of N_2. If we use equation 2.2 to calculate the number of nitrogen molecules arriving at room temperature and 1 torr of pressure, we obtain a value of 3.88 x 10^{20} molecules cm^{-2} s^{-1}. Assuming that a single complete atomic layer (monolayer) of the substrate consists of about 10^{15} cm^{-2} and taking the sticking factor to have a value of one, the time needed to cover the substrate with a complete monolayer of nitrogen under the temperature and pressure conditions mentioned

above is in the order of 1 μs! If we aspire to study at an atomic level the properties of a well characterised adsorbate/substrate system, it is obvious that the composition of the system must stay constant while the experiment is being performed. Without the use of ultra-high-vacuum techniques our system will contaminate even before we start to study it. The result of the previous calculation for a pressure of 10^{-10} torr indicates that under such lower pressure conditions getting one monolayer of contaminants on the surface will take several hours.

The procedure for cleaning a contaminated surface depends on what type of material the surface consists of. A general method to clean a surface is to sputter it by using an ion gun to accelerate rare gas ions against the surface. To restore the ordering of the surface after the sputtering procedure, it is necessary to anneal the sample. The annealing will rearrange the disordered surface atoms to produce an ordered surface. By doing several cycles of sputtering and annealing it is possible to clean most surfaces. A detailed description of the cleaning procedures followed in the preparation of the different surfaces studied in this thesis is given in the corresponding chapters.

There is a further reason why UHV techniques are used in surface science. A considerable number of surface science techniques involve the use of photons and/or electrons. The mean free path of UV and soft X-ray photons and, especially, electrons is so low that the probability that they are absorbed or scattered before they reach either the sample (on their way into the surface) or the analyser (on their way out of the sample) is high. Thus, the use of UHV allows the most common surface science techniques to operate, such as LEED and all the electron spectroscopies.

2.2 The experimental chamber

All the systems studied in this thesis involve gas molecules chemisorbed in solid surfaces. To be able to study these systems with photoelectron diffraction, it is necessary to run the experiments under UHV conditions. Therefore, all the experiments presented here were performed in a stainless steel vacuum chamber. The adequate vacuum (base pressure of the order of 1x10^{-10} mbar) was achieved after careful baking of the system and outgassing of the different filaments and the sample holder, to remove the contaminants adsorbed on their surface. Once the contaminants leave the wall of the chamber, the filaments and the sample holder, they are extracted from the chamber by pumping with a combination of rotary, turbo and titanium sublimation pumps.

Our UHV chamber consists of two chambers connected vertically by a gate valve. The upper chamber was exclusively used for sample preparation. To clean the different single crystal surfaces used in this thesis, they were subject of several cycles of Ar^+ or Ne^+ sputtering followed by thermal annealing (a more detailed description of the cleaning procedure used in each particular case is given in the corresponding chapters). The argon and neon ions were accelerated with an ion gun attached to the upper chamber. A separately pumped gas line was used to fill the chamber with the sputtering gases, and to dose the

different gases used as adsorbates (except in the case of α-alanine, which was dosed with a special home-made doser described in section 5.2.1). A quadrupole mass spectrometer connected to the upper chamber was used for leak testing (performed before the bake out of the chamber) and to check the purity of the different gases utilised in the experiments. The upper chamber was also equipped with standard LEED optics to check the crystallinity of the surfaces before exposure to the adsorbates, and also to characterise the adsorbed overlayers created after dosing. The lower chamber was connected directly to the beamline and, therefore, it was used for all photoemission experiments. The analyser used for recording all the spectra of this thesis was an Omicron EA-125HR 125 mm mean radius hemispherical electrostatic analyser equipped with a seven-channeltron parallel detection system which was mounted in the lower chamber at a fixed angle of 60° to the incident X-radiation in the same horizontal plane as that of the polarisation vector of the linear polarised radiation used in the photoelectron diffraction experiments. All the spectra in the present work were measured in the constant analyser transmission mode. The pressure of each chamber was monitored with corresponding ion gauges. The sample holder was capable of x, y and z motion as well as polar and azimuthal rotations. Sample cooling was achieved via a copper braid connected to a liquid nitrogen cooled cold finger. Heating of the samples was via a filament placed directly behind the back mounting plate of the sample holder.

2.3 Core level photoemission spectroscopy

The criterion that a surface science experimental technique has to fulfil is to have high surface specificity. In macroscopic objects, the number of atoms that are situated at the surface is far less than the total number of atoms contained in the object. Therefore, if all the atoms would contribute equally to the total detected signal measured with a certain experimental technique, surface science would not be possible. In this respect, photoemission spectroscopy satisfies the criterion of being surface specific. In photoemission spectroscopy a photon of a given energy impinges in a surface where it has a certain probability of being adsorbed by an electron. If the photon energy is high enough, this electron can be emitted from the solid. On its way out, the electron can lose energy in a number of ways, which makes it less probable that electrons emitted deeper in the solid will scape and be detected. At the typical electron kinetic energies present in a photoemission experiment, 5-2000 eV, the electron escape depth is in the order of few tens of Å and less. This implies detection of emission from atoms that belong to the outermost atomic layers, which assures the surface specificity of the technique.

For electrons in a solid to be photoemitted into the vacuum, they have to overcome a potential barrier called the *work function*. For metals, the work function is the energy needed to extract an electron from the Fermi level into the vacuum at infinity (that is, far enough from the surface so that it does not feel its electrostatic potential). The major part of this energy is thus independent of the properties of the surface. In addi-

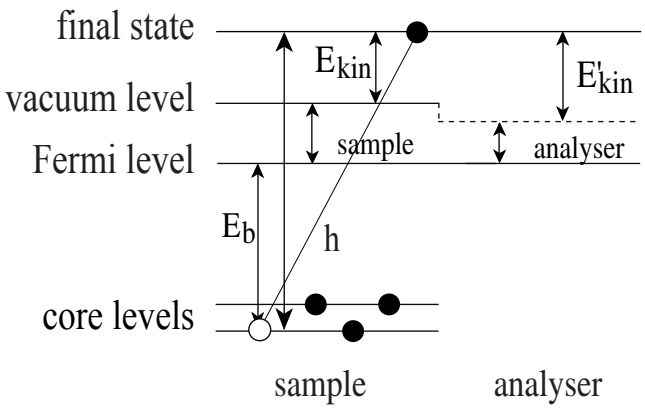

Figure 2.1: Schematic picture of the photoemission process

tion, however, there are surface dipoles associated with spill-over of the electron charge into the vacuum, and due to Smoluchowski smoothing [6], which contribute to the orientation dependence of the work-function. The surface contribution to the work function is markedly influenced by the presence of adsorbates, specially if their electron affinity differs from that of the atoms of the surface. The work function is characteristic for each material, with values of a few eV (that excludes the use in photoemission spectroscopy of near ultraviolet, visible and higher wavelength radiation).

Photoemission spectroscopy can be divided into two different branches depending on the energy of the utilised photons. When photons in the ultraviolet regime (say 5 to 100 eV) are used, electrons in the valence band can be emitted. This type of photoemission spectroscopy is called valence band photoemission spectroscopy or UPS (ultraviolet photoemission spectroscopy). When higher photon energies, in the X-ray regime (>100 eV), are used, then electrons that are in the core levels of an atom can be emitted. In this case we talk about core level photoemission spectroscopy, also called XPS (X-ray photoemission spectroscopy). The additional term SXPS (soft X-ray photoemission spectroscopy) is usually used to refer to core level photoemission spectroscopy carried out at photon energies between 100 and 1000 eV. In this thesis we have only employed core level photoemission spectroscopy in the soft X-ray regime, in which electronic states with low angular momentum (as those measured in this thesis) have usually larger photoionisation cross sections.

Essentially, the kinetic energy of photoemitted electrons from a core level follows the relation:

$$\mathrm{E_b} = \mathrm{h}\nu - \mathrm{E_k} - \phi = \mathrm{E_{final}} - \mathrm{E_{initial}} \tag{2.4}$$

where E_b is the binding energy of the specific level defined relative to the Fermi level, $\mathrm{h}\nu$ is the photon energy, E_k is the kinetic energy of the emitted electrons in the vacuum and ϕ is the work function of the surface. Technically, an electron energy analyser is used to measure the kinetic energy of the outgoing electrons. Therefore the work function of the analyser and the detected kinetic energy of the electrons must replace E_k and ϕ in equation 2.4. This simple view of the photoemission process considers that the remaining electrons

within the atom are not affected by the photoemission process and their corresponding orbitals can, therefore, be considered as *frozen orbitals*. This would then result in only one main line in the photoemission spectrum appearing at the so called Koopman's energy. In reality, however, the ionisation of a core level electron is a more complicated process, and this Koopman's energy is never observed. In the first place, photoemission produces a final state that is lacking one electron with respect to the initial state. The creation of this core hole causes a relaxation of the other electron orbitals, which contract towards the nucleus in order to screen the hole, so that more energy can be available for the outgoing photoelectrons. This leads to a lowering of the photoelectron binding energy (called intra-atomic relaxation shift, E_r), which must be included in 2.4:

$$E_b = h\nu - E_k - \phi + E_r = E_{final} - E_{initial} \tag{2.5}$$

This expression would be perfectly valid if the rearrangement of the electron charge occurred in a shorter time scale than the photoemission process. The process in this case is called *adiabatic*. However, photoemission is usually much faster than the time required for the system to rearrange fully its electron charge distribution. This typically results in a final state which include multiple excitations, involving electrons excited to bound states of the atom or even into the continuum of unbound states above the vacuum level. Such events lead to the occurrence in the core level photoemission spectrum of so called *satellites*. These satellites appear at lower kinetic energies than the *main peak*, also called the *adiabatic peak*. They are usually referred to as *shake-up* and *shake-off* features, depending on whether excitation occurs into a bound state or into the continuum.

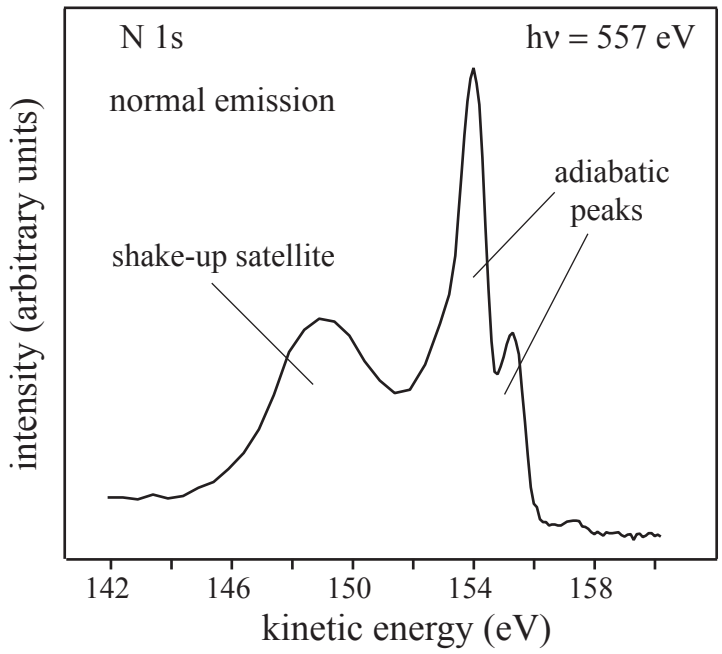

Figure 2.2: N 1s photoemission spectrum from the Ni(100)c(2x2)-N_2 system studied in chapter 3 of this thesis

Fig. 2.2 shows the N 1s photoemission spectrum for the Ni(100)c(2x2)-N_2 system studied in the chapter 3 of this thesis. The broad feature that appear at lower kinetic energy is a satellite associated with several shake-up transitions. The two narrow peaks that appear at higher kinetic energies are associated with main adiabatic emission from the 1s level of the two inequivalent N atoms. The 'energy shift' between the N 1s photoemission components associated with the two inequivalent N atoms in the Ni(100)c(2x2)-N_2 system is a reflection of one of the main characteristic of photoemission spectroscopy: The existence of different local chemical and/or electronic environments gives rise to the appearance in the photoemission spectrum of different components which are shifted in energy. Indeed, this peculiarity, together with the fact that core levels are essentially characteristic in their energy of the atomic species, is what makes core level photoemission spectroscopy such a powerful technique for the chemical charaterisation of adsorbates on surfaces. These energy shifts are called 'chemical shifts', and can also be observed in some cases for emission from the same atomic or molecular adsorbate species at different adsorption sites.

As we can see in Fig. 2.2, the different features that appears in this spectrum are not single lines at a certain energy, but have some energy width. This is intrinsically related to the photoemission process and to the way photoemisison spectra are measured. The first factor to be considered in the broadening of a photoemission peak is the lifetime of the core level, which is a direct reflection of the uncertainty in the lifetime of the ion state remaining after photoemission. Due to this uncertainty, the energy of such a level cannot be precisely determined, but will have an uncertainty of order $\hbar/\tau$. Therefore, there is a certain probability that photons will be emitted with energies $E_b \pm \hbar/2\tau$. This causes a Lorentzian broadening to the peak, which for the broadest core levels (e.g. Ag 3s) is of the order of $\sim$0.1 eV. Another factor that influences the shape of a core level photoemission peak is vibrational broadening. Within a molecule, the removal of a core electron leads to substantial modifications in the electronic structure, which may influence the equilibrium bond distances, or the shape of the potential energy curve. Due to the sudden nature of the photoemission event, the final state is created in the initial state geometry. If the difference in geometry or shape of the potential energy curve between the initial and final state is large, different vibrational modes will be excited in the final state and hence will give rise to additional satellites which are generally not resolvable and this lead to a broadening of the core photoemission peak. The excited intramolecuar vibrations are manifested in the well established vibrational Franck-Condon transitions [7]. Upon adsorption of the molecule on a surface, new vibrational modes may be possible, leading to additional broadening compared to the gas-phase spectrum. These correspond to frustrated rotations and vibrations. To all this, we have to add the experimental energy resolution, which is determined by the energy width of the photon source and the energy analyser resolution (this latter contribution is the same for all peaks when the analyser operates in the constat transmission energy mode).

Energy losses caused by multiple ionisation processes are consider as intrinsic losses. Photoelectrons can also lose some energy on their way to the surface by electron-electron or electron-plasmon interaction (extrinsic losses). In this thesis we deal with adsorbate

emission, so the possible coupling to bulk plasmons can be consider to be weak. Nevertheless, there are examples of adsorbate photoemission peaks showing clear surface plasmon losses, although they are usually seen on rather free-electron-like materials (such as Al, Mg and the alkali metals) which is not the case here (Ni, TiO_2, Cu).

Of course, intrinsic and extrinsic losses that appear too close to the main adiabatic peak to be experimentally resolved, will also contribute to the broadening of a photoemission peak. The same occurs when unresolved chemically shifted photoemission components are present.

Finally, the photoemitted electrons can be scattered off the surrounding atoms. This scattering can be elastic (when the electrons keep their energy after being scattered) or inelastic. The part of the electron wave which is inelastically scattered, loses some energy on its way to the surface, by electron-electron or electron-photon interaction. Once it reaches the detector, gives rise to a continuous background that must be subtracted from the photoemission spectrum before the analysis. The elastically scattered wave interferes in a coherent way with the direct wave. This interference produces photoemission intensities, which vary with emission angle and energy. This is the basis of the photoelectron diffraction technique, as we discuss in the next section.

2.4 Photoelectron diffraction

As already mentioned, the coherent interference between the direct emitted electrons and those elastically scattered off the surrounding atoms, causes variation in the photoemission intensities that depend on the emission angle and energy. The "diffraction pattern" that is obtained in the detector is characteristic of the local geometrical arrangement of the scattered atoms around the emitter, since the path length differences relative to the directly emitted wave component carry information about the position of the emitter relative to the surroundings. Measuring photoelectron diffraction spectra at different energies and emission angles will allow the local structural determination around a particular emitter.

2.4.1 Modes of photoelectron diffraction

Consider the simple scattering process depicted in Fig. 2.4. An electron leaving the emitter (placed at r=0) have a wave function:

$$\psi_{\mathrm{i}}(\mathrm{r}) \sim \frac{\mathrm{e}^{\mathrm{ikr}}}{\mathrm{r}} \tag{2.6}$$

when such a wave arrives to the vicinity of an atom placed at a distance r_j, it can be elastically scattered. Due to this, the final wave function that we will observed at the detector (which is considered to be at an infinite distance from both the emitter and the scatterer) is a combination of the direct wave and the scattered wave given by the

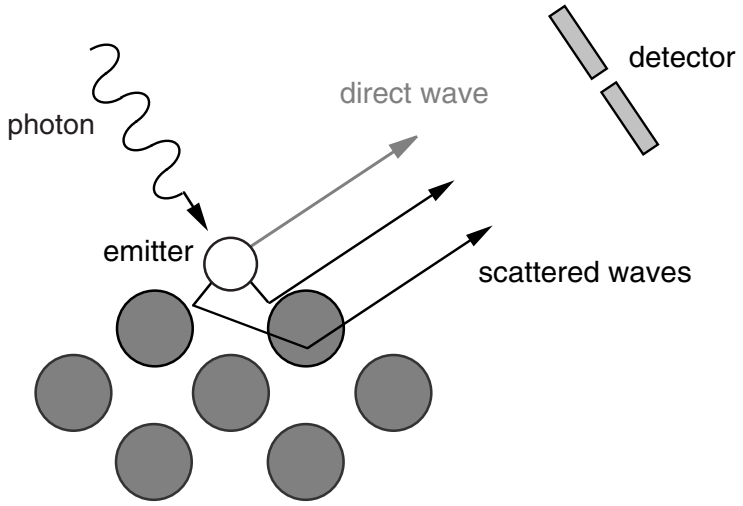

Figure 2.3: Schematic representation of a photoelectron diffraction experiment

expression:

$$\psi_{\mathrm{f}}(\mathbf{r}) \sim \frac{\mathrm{e}^{\mathrm{ikr}}}{\mathrm{r}} \left[1 + \frac{\mathrm{e}^{\mathrm{ikr_j}(1-\cos\Theta_{\mathrm{j}})}}{\mathrm{r_j}} \mathrm{F}(\Theta_{\mathrm{j}}, \mathrm{E}) \right] \tag{2.7}$$

where $F(\Theta_j, E)$ is the so called *elastic scattering amplitude*, which carries the information on the scattering process through its dependence with the scattering potential $\mathrm{V}(\bar{\mathrm{r}}' - \bar{\mathrm{r}}_{\mathrm{j}})$:

$$\mathrm{F}(\Theta_{\mathrm{j}}, \mathrm{E}) = \int \mathrm{d}^3\mathrm{u} \mathrm{e}^{\mathrm{i}(\bar{\mathrm{k}}_{\mathrm{j}} - \bar{\mathrm{k}}_{\mathrm{r}})\bar{\mathrm{u}}} \mathrm{V}(\bar{\mathrm{u}}) \tag{2.8}$$

where $\bar{\mathrm{u}} = \bar{\mathrm{r}}' - \bar{\mathrm{r}}_{\mathrm{j}}$. The elastic scattering amplitude is a complex quantity that is usually written in the form $|\mathrm{F}(\Theta_{\mathrm{j}}, \mathrm{E})| \, \mathrm{e}^{\mathrm{i}\gamma(\Theta_{\mathrm{j}})}$, where $\gamma(\Theta_j)$ is the relative phase of the incoming wave and the scattered one.

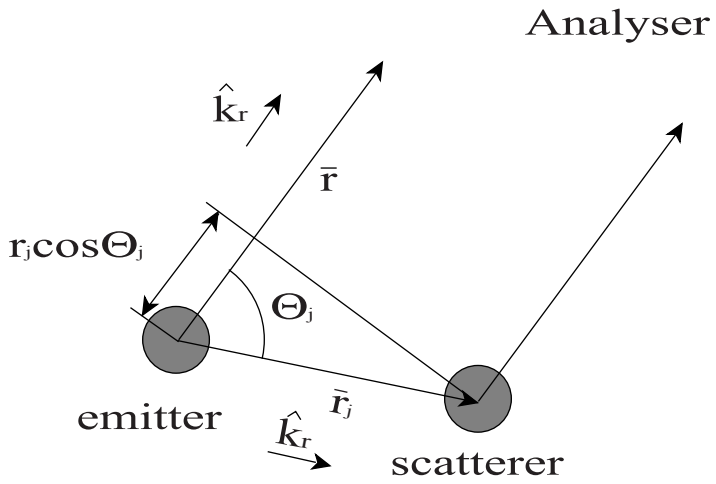

Figure 2.4: Schematic view of a single scattering process

Of course, the scattering process suffered by an electron on the atoms of a surface is more complicated. For a full description of the phenomenon we must take into account not only the single scattering events that the electron will experienced at each of the scatterer atoms, but also the possibility of that the scattered waves can in turn also be scattered. However, the basic underlying physics is the same, and with the help of this simplistic view of the photoelectron diffraction process we can classified the two different modes of operation of this technique.

The modulus of the elastic scattering amplitude is a function of the photoelectron kinetic energy and the scattering angle. Fig. 2.5 shows the variation of this quantity for a Cu atom as a function of the scattering angle for two different photoelectron kinetic energies. From the information contained in this picture we can easily derive the two existing different versions of photoelectron diffraction, which depend on the kinetic energy of the electrons leaving the sample. At high electron kinetic energies (typically above 500 eV) the modulus of the elastic scattering amplitude is dominated by strong forward scattering (i.e., by scattering occurring in the direction of movement of the electron), while at lower energies backscattering becomes of comparable importance. In the high energy case the phase shift involved in the forward scattering event is small. Thus, the interference along the direction of the flying electrons involves zero path length difference between the direct and the scattered waves, leading to a constructive interference. Once we move away from this angle, the scattering amplitude falls, and a path length is introduced, so that the interference is now increasingly destructive. Therefore, at these high electron kinetic energies, the scattering creates a peak in the photoemission signal along the interatomic distance from the emitter to the scatterer, as depicted in the lower left panel of Fig.2.5. This version of photoelectron diffraction is called *scanned-angle mode*, since these experiments consists of measuring the photoemission intensity of a certain core level at a fixed (and high enough) photon energy, while varying the emission angle. Some authors use the acronym XPD (X-ray photoelectron diffraction) to refer to this mode. The use of this version clearly implies that the photoelectron emitter atoms must lie behind the scatterer atoms relative to the detector. For this reason this mode of photoelectron diffraction has been applied most widely to the study of the structure of thin epitaxial films. An advantage of the use of this version is that the interpretation of the data is potentially rather straightforward and often quite good quantitative interpretation can be achieved using simple single scattering simulations. A further advantage of this mode of photoelectron diffraction is that it does not require the use of synchrotron radiation. A commercial X-ray source can be used, which makes this technique accessible to home laboratories.

At low energies (< 500 eV), by contrast, the scattering factor is more isotropic with the angle, although it usually shows peaks in the near-forward and near-backward directions. Bearing in mind that adsorbates typically lie 'above' the surface, using photoelectron diffraction in this energy range, in which backscattering is possible, can provide structural information on the adsorption site. This version of the technique, usually conducted in the *scanned-energy mode*, consists of recording the photoemission spectra at a fixed geometry while the photoelectron kinetic energy is varied. By scanning the photon energy,

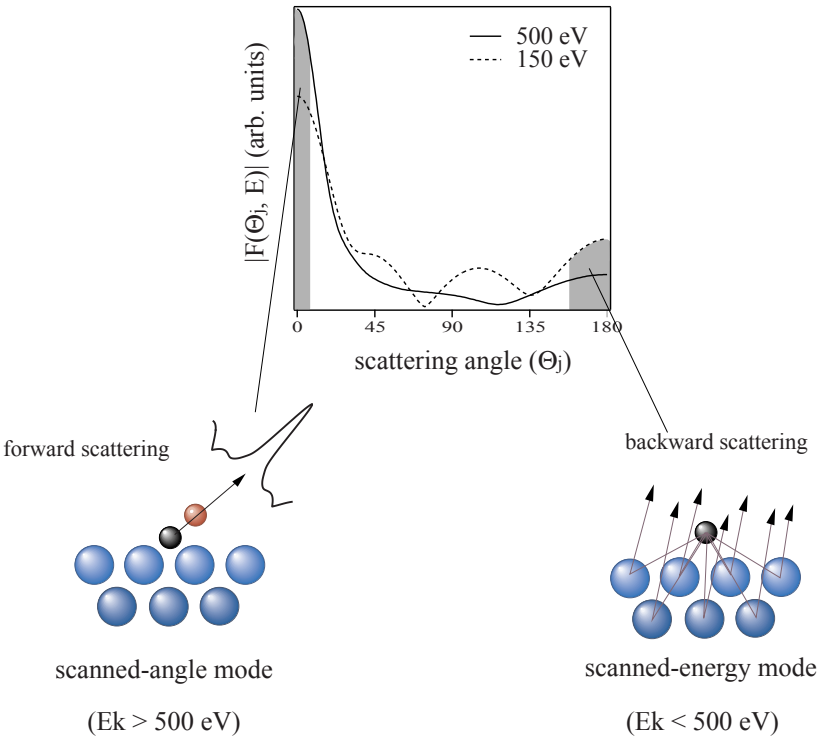

Figure 2.5: Modulus of the elastic scattering amplitude for a Cu atom as a function of scattering angle for two different photoelectron kinetic energies(up); modes of photoelectron diffraction (bottom)

and hence the photoelectron energy and its wavelength, the scattering paths switch in and out of phase leading to intensity modulations which can be interpreted, with the aid of model calculations, in terms of the local emitter geometry. Experimentally, the need for a tunable photoelectron energy requires the use of synchrotron radiation. The interpretation of data is now more complicated, since usually multiple scattering events must be taken into account.

The structural geometries of the three different adsorbate/substrate systems reported in this thesis were determined by using the photoelectron diffraction technique in its scanned-energy mode. The experimental procedure followed in the acquisition of the data, as well as the way they were analysed, are described in the following sections.

2.4.2 Experimental methodology

Our experimental methodology consisted of measuring the photoemission spectrum from a core level of an adsorbed atom (Fig. 2.6.a) at a fixed emission geometry in an photoelectron kinetic energy range of around 300 to 400 eV in energy steps of 3 or 4 eV. The result of such a procedure is shown in Fig. 2.6.b.

Data acquisition for a full PhD spectrum takes about two hours. This procedure is repeated for different emission geometries, so that the final data set comprises the number

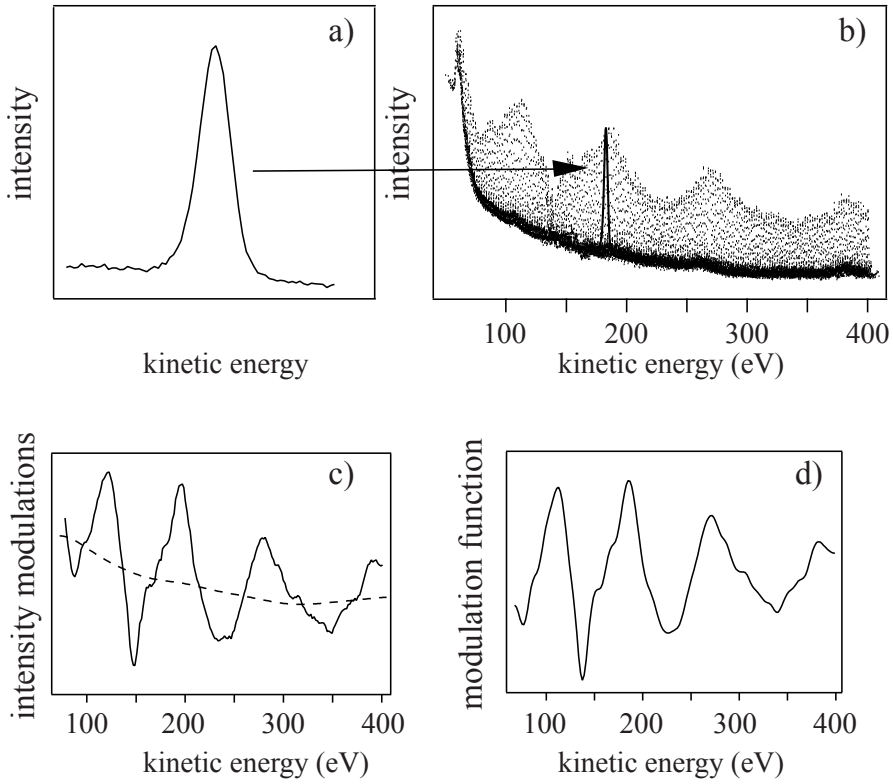

Figure 2.6: a) single photoemission spectrum from a core level of an adsorbed atom; b) photoelectron diffraction spectrum consisting of a series of around 100 photoemission spectra measured at a fixed emission geometry and different kinetic energies; c) result of the integration of a PhD spectrum; d) normalised modulation function (χ(E))

of PhD spectra necessary for a proper analysis. To extract the PhD modulation function from the raw data, the photoelectron intensity is calculated by integration of each of the photoelectron peaks contained in the PhD spectrum (usually around a 100 photoemission spectra). For this purpose a suitable superposition of a Gaussian function and a step with a slope (used to describe the electrons which have gone through small energy loss processes) is fitted to the data after the spectral background has been subtracted. The spectral background is extracted by using the background from the high energy side of each individual photoemission peak. The resulting energy dependence of the photoelectron peak intensities is then plotted as a function of the photoelectron kinetic energy (Fig.2.6.c). The final modulation functions (χ(E)) that will be used in further analysis are obtained after normalising the data to their average values, in order to correct for both the smoothly varying monochromator output flux and the variation of the photoionization cross-section with energy, that is:

$$\chi(\mathrm{E}) = \frac{\mathrm{I}(\mathrm{E}) - \mathrm{I}_0(\mathrm{E})}{\mathrm{I}_0(\mathrm{E})} \tag{2.9}$$

where I_0(E) is obtained from a stiff spline through the intensity I(E).

2.4.3 Structure determination

The next step in the analysis of PhD data is to compare the experimental PhD spectra obtained as described in the previous section with the results of multiple scattering simulations based on a series of 'guessed' structural models until an acceptable fit is achieved. These simulations were performed using a Fortran77 code based on an approach by V.Fritzsche et al. [8–14] and developed by Fritzsche himself. This code run on a cluster of Linux computers combined to create a parallel virtual machine by M.Kittel [15]. The Fritzsche code is based on the expansion of the final state wave-function into a sum over all scattering pathways which the electron can take from the emitter atom to the analyser. A magnetic quantum number expansion of the free electron propagator is used to calculate the scattering contribution of an individual scattering path. Double and higher order scattering events are treated by means of the reduced angular momentum expansion [8]. The finite energy resolution and angular acceptance of the electron energy analyser are accounted for analytically. A more detailed description of the Fritzsche approach can be found in reference [16].

The comparison between theoretical and experimental modulation amplitudes is quantified by the use of an objective reliability factor given by the expression:

$$\mathrm{R} = \frac{\sum_{\mathrm{i}}(\chi_{\mathrm{the}}(\mathrm{E_i}) - \chi_{\mathrm{exp}}(\mathrm{E_i}))^2}{\sum_{\mathrm{i}} \chi^2_{\mathrm{the}}(\mathrm{E_i}) + \chi^2_{\mathrm{exp}}(\mathrm{E_i})} \tag{2.10}$$

such that a value of 0 corresponds to perfect agreement, 1 to no correlation and 2 to anti-correlation. Typically, minimised values of the reliability factor below 0.3 are generally expected for what is thought to be a final true structure.

The multiple scattering simulations include the variation of several structural parameters, the vibrational amplitudes of the emitter and the scatterer atoms, and the real and imaginary parts of the inner potential (to take into account the damping energy off set, and refraction of the electrons). Initial refinement of the structural model is performed by sequential changes of a single parameter in regular steps. This is repeated for all main parameters in the model. Successive optimisation of the model is conducted semi-automatically using a Gauss-Newton algorithm which assumes the shape of the R-factor minimum to be parabolic. For the energy resolution in the present setup it proved sufficient to calculate around 1000 scattering pathways up to third order scattering.

This procedure has an intrinsic weak point. It is clear that without some prior knowledge of the approximate adsorption site, this method would be a tedious and time-consuming enterprise. Furthermore, it could happen that without this prior knowledge we may arrive at an incorrect geometry by optimising to a local best fit quite different from the true structure. It would be a great advantage to have a method of extracting the adsorption geometry directly from the experimental data, if only approximately.

Projection method

The method of direct data inversion used in this thesis to obtain an initial trial model for the structure determination was the so called *projection method* developed by P. Hofmann and K.M. Schindler [17]. At the energies typically used in a photoelectron diffraction experiment, the nearest neighbour backscatterer atom dominates the interference of the direct and the scattered waves when the collection direction is along the backscatterer-emitter bond direction, producing strong long-period modulations. The obvious way to identify this direction is, as proposed by Fritzsche and Woodruff [18], to calculate Fourier transforms of each PhD spectrum (converted from photoelectron energy to photoelectron wave number).

$$\mathrm{u}(\mathbf{r}) = \int \chi_{\mathrm{exp}}(\mathbf{r})\mathrm{e}^{\mathrm{i}\mathbf{kr}}\mathrm{d}\mathbf{k} \tag{2.11}$$

The spectrum having a Fourier transform dominated by a large-amplitude single peak would be the one taken in a geometry most nearly aligned along the emitter-near backscatterer direction.

While this method allows one to identify the position of the emitter atom relative to the surrounding scatterer atoms, it does not give reliable information about the actual interatomic distances. This question was solved by Hofmann and Schindler. At the near-backscattering geometry, the main contribution to the PhD spectra comes from the single backscattering events. Therefore, if in the standard Fourier function we replace the pure harmonic phase function by a theoretical single scattering modulation function calculated for a scatterer atom placed at a certain position below the emitter, the match of an experimental spectrum and this single scatterer modulation function calculated in the same emission direction can be expressed in the form of a projection coefficient define by:

$$\mathrm{c}(\mathbf{r}) = \int \chi_{\mathrm{exp}}(\mathbf{k})\chi_{\mathrm{the}}(\mathbf{r},\mathbf{k})\mathrm{d}\mathbf{k} \tag{2.12}$$

where $\mathbf{k}$ is the wavevector of the outgoing electron. The values of the projection coefficients for the different experimental emission directions are then combined in an exponential summation:

$$\mathrm{C}(\mathbf{r}) = \sum_{\mathrm{i}} \mathrm{e}^{|\mathbf{r}|\mathrm{c_i}(\mathbf{r})} \tag{2.13}$$

and this quantity is calculated for different positions over two-dimensional grids below the emitter and the results displayed as grey-scale maps with the darkest areas corresponding to the highest values of $\mathrm{C}(\mathbf{r})$. When the test site $\mathbf{r}$ corresponds approximately to the position of a backscattering substrate atom, the value of $\mathrm{C}(\mathbf{r})$ will be greatest, with high contrast due to the exponential nature of the summation in equation 2.13. One important requirement for this to hold is that a PhD spectrum in (or very close to) the backscattering emission direction is to be included in the data set. Thus, maps of the $\mathrm{C}(\mathbf{r})$ values can be interpreted (in favourable circumstances) as images of the substrate backscatterers around the emitter. The lower panels of Fig. 2.7 show the application of this method to an adsorbed atom on a four-hollow adsorption site.

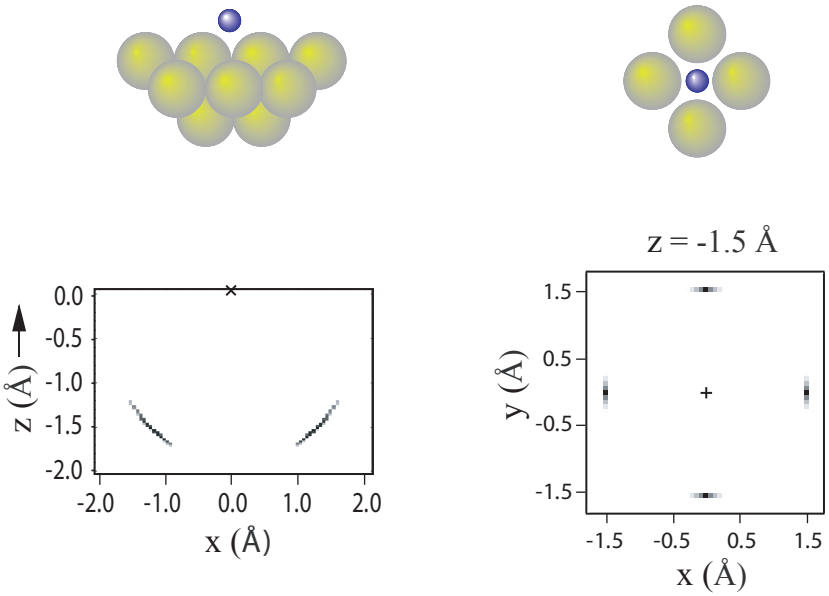

Figure 2.7: Results of applying the projection method to PhD data from an atom adsorbed in a four-hollow site at approximately 1.5 Å above the surface

The projection method is designed to be applicable only to elemental substrates, for which all scatterers are assumed to have the same scattering phase shifts. Therefore, we could not use it in the study of the adsorption of formic acid on $TiO_2(110)$.

Estimation of errors

Once the correct adsorption geometry has been found, we must quantify the significance of the results by estimating their associated errors. The approach used in photoelectron diffraction derives directly from that used by Pendry for estimating errors in LEED (low energy electron diffraction) [19], which is based on the assumption that deviations between measured and calculated PhD spectra are exclusively statistical.

The range of acceptable values for a given parameter are those within the variance of the minimum of the reliability factor, which is given by:

$$\mathrm{Var}(\mathrm{R_{min}}) = \mathrm{R_{min}}\sqrt{\frac{2}{\mathrm{N}}} \tag{2.14}$$

where N is the number of independent pieces of structural information contained within the data set used for evaluation. According to Pendry's definition, this is the maximum number of peaks which could occur over a given energy range. N is limited by the natural line width of the peaks which is in turn determined by the damping of the electron waves within the crystal potential. This damping is determined by the imaginary part of the optical crystal potential. In LEED the line width is taken to be $4|V_{0i}|$. In photoelectron diffraction the peak widths are also limited by the effects of energy resolution which

attenuate the contributions of distant scatterers. Therefore, in the multiple scattering calculations the energy broadening is entered explicitly. Hence, the estimate of the minimum width of the peaks is given by the quadrature sum of the imaginary part of the inner potential and energy broadening factor E_b:

$$N = \frac{\delta E}{4\sqrt{V_{oi}^2 + E_b^2}} \tag{2.15}$$

2.5 Synchrotron radiation

As commented above, photoelectron diffraction in the scanned-energy mode requires the use of synchrotron radiation. Synchrotron radiation is produced when charged particles moving at relativistic velocities are accelerated. It is a well known phenomenon that an accelerated charged particle emit radiation. But why does it so? Consider a charged particle which is either at rest or in uniform motion through vacuum (i.e. in absence of external electromagnetic fields). This charged particle creates electric field lines that are either at rest or moving uniformly together with the particle. Now imagine that the particle suffers a sudden acceleration for a short period of time (such as the one caused by the sudden presence of a magnetic field). This implies that the electric field lines created by the charged particle are also accelerated. This change is perceived almost instantaneously in the vicinity of the particle, so the field lines continue to point radially to it. Far away from the charged particle, however, the field lines are still directed towards the position where the particle would had been, if it were not have been accelerated (this is a direct consequence of the finite velocity of light). Somewhere between these two distances, the field lines will be distorted, and it is this distortion travelling away from the charged particle at the velocity of light that is called electromagnetic radiation. A mathematic explanation of this phenomenon can be obtained from the Maxwell equations for dynamic fields.

As the speed of a charged particle approaches the speed of light, its radiation pattern appears (due to relativistic effects) to the observer in the laboratory as being all emitted in a narrow cone along the instant direction of motion of the particle. When charged particles move at these relativistic velocities, they radiate from the IR (infrared) into the near X-ray regime, and this radiation is called *synchrotron radiation*.

In a synchrotron radiation facility like that of BESSY II[1], where all the data of this thesis were measured, the electrons are primarily accelerated to relativistic velocities before they are injected in the so called storage ring. This acceleration process is carried by the action of a external accelerator (usually a combination of linear and synchrotron accelerators). Once in the storage ring, the electrons are accelerated to their final energy (1.7 GeV in the case of BESSY II) by the alternating field of a cavity resonator. Strong bending and focusing magnets are used to keep the electrons in a closed orbit inside the

[1]Berliner Elektronenspeicherring-Gesellschaft für Synchrotronstrahlung mbH (BESSY II) in Berlin, Germany [20]

storage ring. Electrons radiate when they pass through these bending sections. Bending magnet radiation is directed tangentially outward from the electron trajectory in a narrow radiation cone with an opening angle given by $\gamma = mc^2/E_e$, where E_e is the energy of the radiating electron. The radiation spectrum for bending magnets is very broad, analogous to a "white light" X-ray light bulb. To generate more intense synchrotron radiation, third

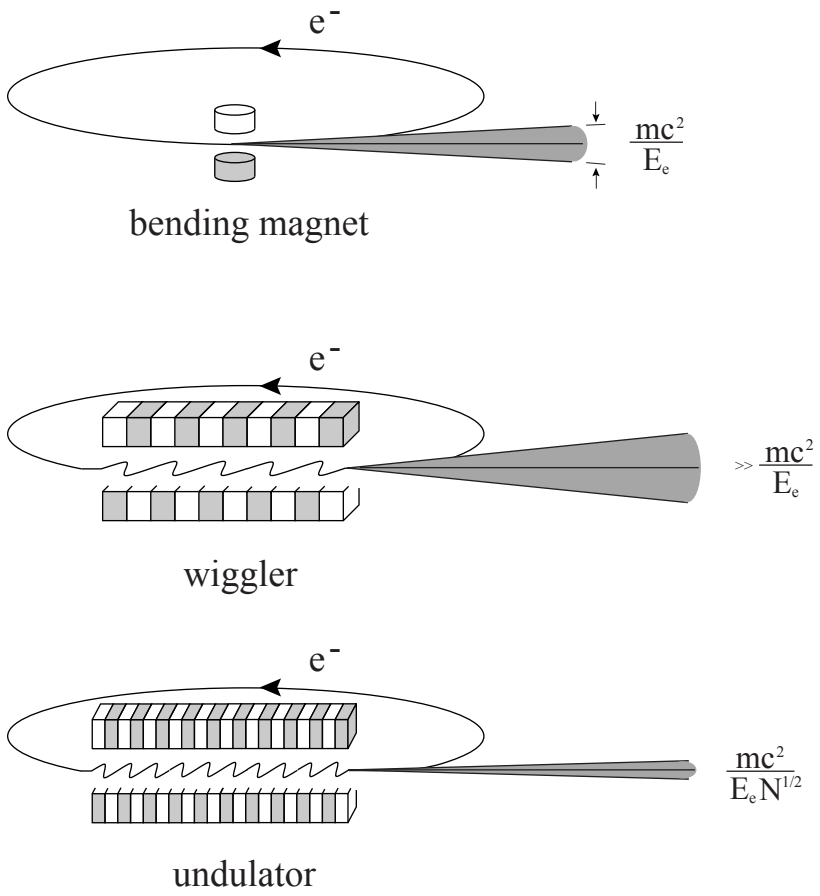

Figure 2.8: Synchrotron radiation from a bending magnet (top), a wiggler (middle) and an undulator (bottom)

generation storage rings (like BESSY II) contain other devices, the so called *insertion devices*, which are placed in magnet free sections of the orbit. The insertion devices most commonly used are multipole wigglers and undulators [2]. These devices consist of a periodic array of magnets with alternating polarity, such as depicted in Fig. 2.8. When a relativistic electron passes through these devices, it changes its trajectory at every magnet, resulting in a oscillatory motion characterised by small angular paths. In each of these curved deflections, the electron emits radiation in the same forward direction. The radiation emitted at each magnet adds up along the device to produce a more intense signal at the end. The difference between the light obtained with a wiggler or with an undulator is

[2]BESSY II also has wavelength shifters which are wigglers with just a few-magnets with a extremely high field in the central pole whose purpose is to shift the spectrum towards the hard x-rays region

caused by the strength of the magnetic field generated by the magnets in either case. In a wiggler, the magnetic field of each magnet is so strong, that it bends the electron beam through a large angle compared with the angular width of the natural radiation cone normally associated with synchrotron radiation(γ). This produces high intensity broad band radiation, up to photon energies which can greatly exceed those available from the bending magnets. The radiation originated in a wiggler is very broad, similar to that of a bending magnet, but is more intense (2N times as intense due to repetitive electron bending over the N magnets of the wiggler), and also less brilliant[3], because of the substantially increased radiation cone. In an undulator, the magnetic field is relatively weak and the resultant angular paths are smaller than mc^2/E_e. The radiation emitted at the various magnets of the undulator interferes coherently, resulting in radiation of high brilliance which is quasi-monochromatic, peaked in narrow energy bands at the harmonics of the fundamental energy. The spectrum obtained from a undulator is therefore different from the smooth, continuous spectrum produced by a bending magnet or a wiggler.

The synchrotron radiation from bending magnets and conventional insertion devices is linearly polarised in the orbital plane of the storage ring. Left or right circular polarised radiation, as well as elliptically polarised radiation, can be obtained with special magnet structure such as the Sasaki undulator (see [21] for details) in the UE56/2 beamline at BESSY II.

The synchrotron radiation produced either from bending magnets, or from insertion devices, can be used in the experimental stations connected to them, the so called beam lines. In a beam line, a monochromator is used to select a certain band pass of wavelengths out of the emitted spectrum. A set of optical elements is placed along the beam line to transfer as completely as possible the brilliance of the source to the experimental chamber, which is placed at the end of the beamline.

Electrons lose energy as they emit synchrotron radiation. In order to restore this energy lost, the electrons are accelerated each time they pass through the RF (radio frequency) cavity (or cavities) placed in the storage ring. Only the electrons that entry the RF cavity in phase with the sinusoidal field existing there, are accelerated. This causes the electrons to have a time structure that consists of buckets filled with electrons (every of these buckets is called a bunch). Electrons outside a bucket are scattered by the out of phase cavity excitation and are lost.

All the different parts of a synchrotron facility (from the accelerators to the beam lines) are kept at ultra-high-vacuum (of around 10^{-10} Torr) to avoid collisions between electrons and residual gas molecules. Even at such a low pressures, some of these collisions do occur, and the direction and kinetic energy of the electrons are changed. As a consequence, the total number of electrons decreases as a function of time, which makes it necessary to refill the storage ring with electrons every few hours.

All the measurements of the present work were performed using synchrotron radiation from the undulators at beam lines UE56/2-PGM1 and U49-1 (which has been recently

[3] *brilliance* is defined as the photon flux per unit transverse phase-space area

substituted by an UE125 undulator). Besides the tunability of these sources, other great advantages are the high photon flux provided (photon fluxes of around 10^{11} where used in our experiments) and the high energy resolution (in the order of 8000 E/ΔE in our experiments) which can be achieved in the monochromator.

2.6 Overlayer structures and LEED patterns

If the resulting structure of the adsorbate-substrate system is ordered (as in the systems studied in this work), this order is usually described by relating its Bravais lattice to that of the underlying solid. The more general way to do this is to write the primitive translation vectors of the surface unit mesh ($\mathbf{a}'$,$\mathbf{b}'$) as a linear combination of those of the corresponding plane of the underlying substrate ($\mathbf{a}$,$\mathbf{b}$), so that:

$$\begin{aligned} \mathbf{a}' &= p_1 \cdot \mathbf{a} + q_1 \cdot \mathbf{b} \\ \mathbf{b}' &= p_2 \cdot \mathbf{a} + q_2 \cdot \mathbf{b} \end{aligned} \tag{2.16}$$

The overlayer can therefore be specified by the matrix:

$$\begin{pmatrix} p_1 & q_1 \\ p_2 & q_2 \end{pmatrix} \tag{2.17}$$

Notice that the vectors of the substrate (overlayer) are always chosen so that $|\mathbf{a}| \leq |\mathbf{b}|$ ($|\mathbf{a}'| \leq |\mathbf{b}'|$), the angle between them is $\geq 90°$, and the coordinate system is right-handed.

Another notation commonly found in the literature is that in which the ratio of the lengths of the surface and substrate nets is given, together with the angle through which one mesh needs to be rotated in order to have its primitive translation vectors aligned with those of the other mesh. In this notation, the overlayer structured is labelled by (pxq)R$\phi°$, where p = $|\mathbf{a}'| \,/\, |\mathbf{a}|$, q = $|\mathbf{b}'| \,/\, |\mathbf{b}|$ and ϕ is the angle the substrate lattice vectors must be rotated to match those of the overlayer. In addition, those surface structure that can be described with square or rectangular lattices and have two atoms per unit cell, having the second atom in the centre of the square or the rectangle, are usually denoted as c(pxq), where c means centered, and p and q satisfies the relations $\mathbf{a}'$ = p·$\mathbf{a}$, $\mathbf{b}'$ = q·$\mathbf{b}$

In the following we will see how the different notations apply in a particular case. Lets take as example a LEED pattern similar to that shown by the system formed after the adsorption of molecular nitrogen on a Ni(100) surface (see Fig. 2.9).

We have already referred to this structure as a c(2x2), but it can be easily seen that according with the other two notations explained above, this structure can be described as a ($\sqrt{2}$ x $\sqrt{2}$)R45° or via the matrix:

$$\begin{pmatrix} 1 & 1 \\ -1 & 1 \end{pmatrix} \tag{2.18}$$

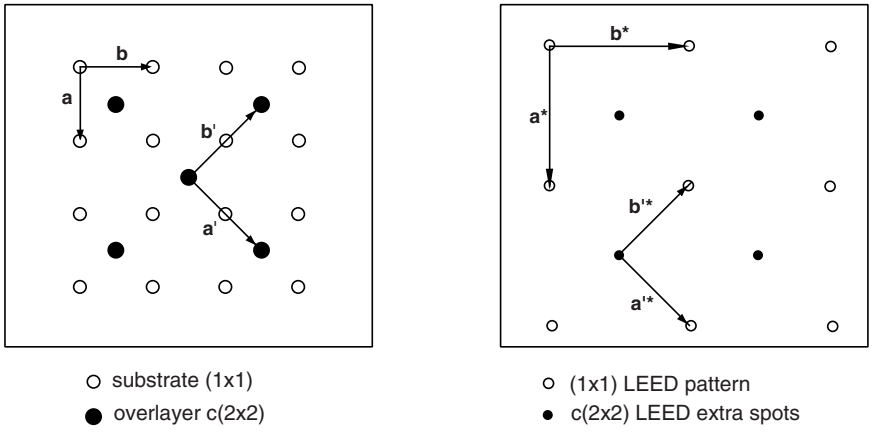

Figure 2.9: c(2x2) overlayer structure and its corresponding LEED pattern

The most convenient way to refer to more complicated overlayers is the matrix notation. This is the notation we use in chapter 5 to describe the overlayer formed by the adsorption of alanine on Cu(100), although instead of writing the corresponding matrix, we quoted this matrix as (p_1 q_1, p_2 q_2).

To check the crystallographic order and quality of the surfaces used in the distinct experiments previous their exposure to the adsorbates, as well as to characterise the long range order of the adsorbed overlayers we made use of another surface sensitive technique as a supporting tool, the low energy electron diffraction technique (LEED). In a LEED experiment, impinging electrons from a monochromatic beam (which energy typically lies within the range of ∼20-300 eV, so that their de Broglie wavelengths are comparable to the interatomic distances) are elastically scattered by the regular array of atoms conformed by the surface. The interference between elastically scattered waves gives rise to a well-defined diffraction pattern in which the positions of the intensity maxima (which appear as spots in a luminescent screen that acts as a detector) are related to the long range periodicity of the lattice. Thus, LEED is very sensitive to the ordering of surfaces. LEED gives information about the translational symmetry of the system in the reciprocal space, but it is rather readily to obtain information about the real space by using the expressions which relate the primitive translation vectors of the reciprocal lattice ($\mathbf{a}^*$ and $\mathbf{b}^*$) to those of the real lattice ($\mathbf{a}$ and $\mathbf{b}$):

$$\mathbf{a}^* = 2\pi\frac{\mathbf{a}\mathrm{x}\mathbf{n}}{\mathbf{a}\cdot\mathbf{b}\mathrm{x}\mathbf{n}}, \qquad \mathbf{b}^* = 2\pi\frac{\mathbf{b}\mathrm{x}\mathbf{n}}{\mathbf{a}\cdot\mathbf{b}\mathrm{x}\mathbf{n}} \tag{2.19}$$

where $\mathbf{n}$ is a unit vector normal to the surface.

In chapter five the concept of *glide plane* is used. A glide plane is a symmetry plane perpendicular to the surface other than those associated with centred nets. When a structure possesses such a plane and both incident and diffracted beams lie in it, the alternate beams for which the indexing is odd are missing along this particular plane.